OPEN

Original article

Nuclear Medicine Communications

Comparison of reprojected bone SPECT/CT and planar bone scintigraphy for the detection of bone metastases in breast and prostate cancer

Samuli Arvola[a], Marko Seppänen[a], Simona Malaspina[a], Sorjo Mätzke[b], Juho Raiko[a], Kirsi L. Timonen[c], Otto Ettala[d], Ivan Jambor[e,f], Mikael Anttinen[d], Anna Kuisma[g], Eliisa Löyttyniemi[h], Peter J. Boström[d], Antti Sohlberg[i,j] and Tommi Noponen[a,k]

Objective **The aim of this study was to compare reprojected bone SPECT/CT (RBS) against planar bone scintigraphy (BS) in the detection of bone metastases in breast and prostate cancer patients.**

Methods **Twenty-six breast and 105 prostate cancer patients with high risk for bone metastases underwent ^{99m}Tc-HMDP BS and whole-body SPECT/CT, 1.5-T whole-body diffusion-weighted MRI and ^{18}F-NaF or ^{18}F-PSMA-1007 PET/CT within two prospective clinical trials (NCT01339780 and NCT03537391). Consensus reading of all imaging modalities and follow-up data were used to define the reference standard diagnosis. The SPECT/CT data were reprojected into anterior and posterior views to produce RBS images. Both BS and RBS images were independently double read by two pairs of experienced nuclear medicine physicians. The findings were validated against the reference standard diagnosis and compared between BS and RBS on the patient, region and lesion levels.**

Results **All metastatic patients detected by BS were also detected by RBS. In addition, three metastatic patients were missed by BS but detected by RBS. The average patient-level sensitivity of two readers for metastases was 75% for BS and 87% for RBS, and the corresponding specificity was 79% for BS and 39% for RBS. The average region-level sensitivity of two readers was 64% for BS and 69% for RBS, and the corresponding specificity was 96% for BS and 87% for RBS.**

Conclusion **Whole-body bone SPECT/CT can be reprojected into more familiar anterior and posterior planar images with excellent sensitivity for bone metastases, making additional acquisition of planar BS unnecessary.**

Nuclear Medicine Communications 2022, **43**:510–517

Keywords: bone, bone scintigraphy, reprojected, SPECT/CT

[a]Department of Clinical Physiology, Nuclear Medicine and Turku PET Centre, Turku University Hospital and University of Turku, Turku, [b]Clinical Physiology and Nuclear Medicine, Helsinki University Hospital, Helsinki, [c]Department of Clinical Physiology and Nuclear Medicine, Hospital Nova of Central Finland, Jyväskylä, [d]Department of Urology, [e]Department of Diagnostic Radiology, Turku University Hospital and University of Turku, Turku, Finland, [f]Department of Radiology, Icahn School of Medicine at Mount Sinai, New York, New York, USA, [g]Department of Oncology and Radiotherapy, [h]Department of Biostatistics, University of Turku, Turku, Finland [i]HERMES Medical Solutions, Strandbergsgatan 16, Stockholm, Sweden [j]Laboratory of Clinical Physiology and Nuclear Medicine, Päijät-Häme Central Hospital, Lahti and [k]Department of Medical Physics, Turku University Hospital, Turku, Finland

Correspondence to Samuli Arvola, MSc, Department of Nuclear Medicine Turku University Hospital, Kiinamyllynkatu 4-8, P.O. Box 52, FI-20521 Turku, Finland
Tel: +358 403293503; e-mail: samuli.arvola@tyks.fi

Received 6 October 2021 **Accepted** 28 December 2021

Introduction

Planar bone scintigraphy (BS) has been the routine method for detection of bone metastases in breast and prostate cancer patients for decades [1]. However, whole-body single-photon emission computed tomography integrated with X-ray computed tomography (SPECT/CT) is gaining usage as it is more sensitive and specific than BS alone for the detection of bone metastases [2]. Also, quantitation using standardized uptake values is feasible in bone SPECT/CT [3,4]. The transition from planar BS to a routine whole-body SPECT/CT workflow seems thus probable in the near future [5]. Some nuclear medicine physicians may still feel reluctant to switch to the more complex and time-consuming reading of multi-slice whole-body SPECT/CT and abandon the familiar methodology of BS. The acquisition of both BS and whole-body SPECT/CT in a row during this transition period might be feasible, but it greatly increases the examination time.

Software algorithms play an important role in SPECT/CT image formation, while BS algorithms are more straightforward. Whole-body SPECT/CT image processing techniques have advanced greatly during the last decade [6]. In this paper, we use commercially available vendor-neutral SPECT reconstruction software to reproject

bone SPECT/CT images, making them appear like traditional BS images. These reprojected bone SPECT/CT (RBS) images could help during the transition from BS to more comprehensive whole-body bone SPECT/CT. By utilizing RBS images, nuclear medicine physicians would be provided with a more familiar planar image along with the tomographic image for the interpretation without the need for additional scanning.

In addition to a familiar planar appearance, RBS could have several other benefits. First, RBS could be more sensitive than BS for changes in bone metabolism due to data corrections included in SPECT/CT reconstruction. Second, unlike BS images, RBS images do not require additional scanning as they are calculated from SPECT/CT images. Third, RBS can be calculated from different angles over 360° rotation [7], suggesting it as a physically more accurate replacement for maximum intensity projection (MIP) images currently used in a rough visualization of SPECT. Finally, RBS images could speed up the reading process of SPECT/CT.

Little evidence of RBS exists in the literature. The usage of reprojected SPECT has been previously validated for lung imaging [8,9], but for now, to our knowledge, its application for bone imaging has only appeared in a conference article [10] and as an image of the month in the *European Journal of Nuclear Medicine and Molecular Imaging* [7]. In this paper, we test the RBS method for the detection of bone metastases in primary staging of high-risk breast and prostate cancer patients. The results of RBS are compared against traditional BS and multimodal reference standard to validate RBS method in a clinical patient cohort.

Materials and methods

Patients

A total of 131 patients were included in this study cohort by combining two patient populations from two prospective clinical trials (NCT01339780 and NCT03537391) [11,12]. The first population consisted of 26 breast and 27 prostate cancer patients prospectively enrolled between February 2011 and March 2013, and the second population consisted of 78 prostate cancer patients enrolled between March 2018 and June 2019. All patients were considered to be at high risk for bone metastases. Detailed patient inclusion criteria are previously published [11,12]. The criteria included suspicious laboratory or histopathologic findings and localized pain in the skeletal area suggesting bone metastases.

All procedures performed in studies involving human participants were in accordance with the ethical standards of the institutional research committee and with the 1964 Helsinki declaration and its later amendments or comparable ethical standards. Informed consent to participate was obtained from all individual participants included in the study.

Patient imaging and reference standard

All patients underwent ^{99m}Tc-HMDP BS, SPECT/CT, and 1.5-T whole-body diffusion-weighted MRI (DW-MRI) for primary metastasis staging. In addition, the first patient population underwent ^{18}F-NaF PET/CT imaging, and the second population ^{18}F-PSMA-1007 PET/CT and contrast-enhanced CT imaging of the thorax, abdomen, and pelvis. The examinations in each patient were performed within 14 days, and the patients were followed for at least 6 months, as previously reported [11,12].

The findings of each imaging modality were compared with the best valuable comparator to define their nature [13–16]. Consensus reading of all imaging modalities and follow-up data of clinical, imaging and laboratory results were used to define the best valuable comparator, which was used as the reference standard diagnosis in the current study. The reference standard diagnosis was mostly on the basis of whole-body DW-MRI and ^{18}F-NaF or ^{18}F-PSMA-1007 PET/CT images.

Bone scintigraphy and SPECT/CT image acquisition

The patients received an intravenous injection of 670 MBq of ^{99m}Tc-HMDP, and BS was started three hours after the injection. The first patient population was scanned using a Symbia T6 True Point SPECT/CT system (Siemens Healthineers, Erlangen, Germany) with low-energy high-resolution collimators, continuous acquisition with scan speed 13 cm/min and a matrix size of 256 × 1024. The second patient population was scanned using a GE Discovery NM/CT 670 CZT system (GE Healthcare) with wide-energy high-resolution collimators, step-and-shoot acquisition, five-bed positions, 3 min per bed position, and a matrix size of 256 × 1024.

A three-bed-position whole-body SPECT was performed from the top of the head to the middle femurs immediately after BS. The acquisition parameters for the first patient population were 180 projections over 360°, 9 s of acquisition time per view, a 128 × 128 matrix, and a 15% energy window centered at 140 keV. The acquisition parameters for the second patient population were the same, except for 120 projections over 360° with a 13-s acquisition time per view. For all patients, the SPECT imaging was followed by a low-dose attenuation-correction CT from the top of the head to the mid-thigh.

SPECT and reprojected bone SPECT/CT image processing

The acquired SPECT data were resampled such that the resulting data represented optimized SPECT acquisition completed within the standard time allocated for planar bone scans at our department. The data from the GE Discovery NM/CT 670 CZT system was acquired in listmode, and it was resampled using the Lister software of the Xeleris 4.0 workstation (GE Healthcare,

Tirat Hacarmel, Israel). The data from the Symbia T6 True Point SPECT/CT system was Poisson resampled using the HybridRecon-Oncology software (version 3.2, HERMES Medical Solutions AB, Stockholm, Sweden). After resampling, the number of counts in RBS images was comparable to that of BS images.

The SPECT data were reconstructed with the HybridRecon-Oncology software (version 3.2, HERMES Medical Solutions AB) using the ordered-subset expectation-maximization algorithm [17] with 6 iterations and 15 subsets and corrections for photon attenuation, scatter, and collimator response [18]. RBS images corresponding to traditional anterior and posterior views of BS were generated by forward projecting the reconstructed three-bed SPECT data. The forward projector of the Hermes HybridRecon reconstruction algorithm traces photons to anterior and posterior detector positions through the CT-based attenuation map used in SPECT reconstruction. CT is therefore mandatory to create RBS images. The RBS images were filtered using a Gaussian filter with 7-mm full width at half maximum.

Data analysis

All BS and RBS images were independently double read by two pairs of experienced nuclear medicine physicians. The physicians were blinded to the results of the other imaging modalities and only informed that the patients had breast or prostate cancer at high risk for bone metastases. Typical benign lesions included uptake around joints, H-shaped pelvic uptake, and uptake extending vertically over several ribs suggesting fracture. Intense focal uptake on skull, sternum, scapula, vertebra, pelvis, rib cage or extremities were considered bone metastases. If the reader was unsure, the lesion was reported equivocal. Similar criteria have also been used in our previous studies [11,12].

The findings were compared at patient-, region-, and lesion-level against the reference standard diagnosis [11,12] to create true positive and negative, and false positive and negative classes. The comparisons were performed using optimistic and pessimistic analyses. In the region-level analysis, the skeleton was divided into six regions: skull, spine, ribs, pectoral girdle and sternum, pelvis, and limbs.

The readers also visually evaluated the overall image quality of each image on a five-point scale: 1 = insufficient image quality, 2 = almost sufficient image quality, 3 = sufficient image quality, 4 = good image quality and 5 = excellent image quality for diagnosis. Quantitative quality of BS and RBS images was measured in a randomly chosen sample of 20 patients. Circular regions of interest (ROI) with 15-mm diameter were placed in BS and RBS images on a normal-appearing femur, lumbar vertebra, the tenth rib, and adjacent soft tissue. Mean and SD of counts in bone and soft tissue ROIs were defined, and contrast-to-noise ratios (CNR) were calculated as

$$CNR = \frac{ROI_{bone,mean} - ROI_{soft\ tissue,mean}}{\sqrt{ROI_{bone,SD^2} + ROI_{soft\ tissue,SD^2}}},$$

where $ROI_{bone,\ mean}$ and $ROI_{soft\ tissue,\ mean}$ are means of counts and $ROI_{bone,\ SD}{}^2$ and $ROI_{soft\ tissue,\ SD}{}^2$ are squared SDs of counts in bone and soft tissue ROIs, respectively.

Statistical analysis

Statistical analyses were performed using the MedCalc statistical software (version 19.2.6, MedCalc Software Ltd, Ostend, Belgium). The sample size estimation was on the basis of the expectation that the sensitivity of RBS would be better than 60%, the approximated sensitivity of BS. Therefore, the lower limit of the confidence interval of RBS sensitivity should be greater than 60% (one-sided, alpha-level 0.05). When the sensitivity of RBS was evaluated to be approximately 70%, which is the minimum expected sensitivity of SPECT, then a statistical power of 80% required 130 patients to be included in the study.

The sensitivity and specificity of BS and RBS were compared at patient and region level using a two-sided McNemar test. Area under receiver-operating characteristic curve (AUC) values were calculated using the trapezoid rule and compared between BS and RBS using the method of Hanley and McNeil [19]. Inter-reader agreement at patient level was evaluated using Cohen's kappa calculations. The values are reported with a 95% confidence interval (CI). *P* values <0.05 (two-tailed) were considered statistically significant. Equivocal lesions were omitted as benign lesions in the optimistic analysis and included as metastases in the pessimistic analysis.

Results

A total of 34 patients out of 131 had skeletal metastases according to the reference standard diagnosis, 103 metastases were located in different skeletal regions, and altogether 163 lesions were considered as positive for bone metastases. The optimistic analysis revealed little difference between the diagnostic performance of BS and RBS, but the pessimistic analysis showed RBS to be a more sensitive but less specific method than BS (Tables 1 and 2). The average patient-level sensitivity of two readers in the pessimistic analysis was 75% for BS and 87% for RBS, and the corresponding specificity was 79% for BS and 39% for RBS. The average region-level sensitivity of two readers in the pessimistic analysis was 64% for BS and 69% for RBS, and the corresponding specificity was 96% for BS and 87% for RBS.

Two patients were correctly reported positive by both RBS readers but falsely reported negative by one BS reader and equivocal by the other. Three patients were falsely reported negative by both BS readers but reported equivocal by at least one RBS reader. Seven patients were correctly reported negative by both BS readers but falsely

Table 1 **Patient-level analysis**

	Optimistic analysis			
	Sensitivity (95% CI)	Specificity (95% CI)	Accuracy (95% CI)	AUC (95% CI)
BS 1	53% (35–70%)	99 % (94–100%)	87 % (80–92%)	0.76 (0.68–0.83)
BS 2	62% (44–78%)	97% (91–99%)	88% (81–93%)	0.79 (0.71–0.86)
RBS 1	65% (46–80%)	92% (84–96%)[a]	85% (77–90%)	0.78 (0.70–0.85)
RBS 2	62% (44–78%)	93% (86–97%)	85% (77–90%)	0.77 (0.69–0.84)
	Pessimistic analysis			
	Sensitivity (95% CI)	Specificity (95% CI)	Accuracy (95% CI)	AUC (95% CI)
BS 1	71% (53–85%)	82% (73–89%)	79% (71–86%)	0.77 (0.68–0.84)
BS 2	79% (62–91%)	75% (65–83%)	76% (68–83%)	0.77 (0.69–0.84)
RBS 1	85% (69–95%)	47% (37–58%)[a,b]	57% (48–66%)	0.66 (0.58–0.74)[b]
RBS 2	88% (73–97%)[a]	30% (21–40%)[a,b]	45% (36–54%)	0.59 (0.50–0.68)[a,b]

AUC, area under receiver-operating characteristic curve; BS 1, bone scintigraphy reader 1; BS 2, bone scintigraphy reader 2; CI, confidence interval; RBS 1, reprojected bone SPECT/CT reader 1; RBS 2, reprojected bone SPECT/CT reader 2.
[a]Statistically significant difference ($P < 0.05$) compared with BS 1.
[b]Statistically significant difference ($P < 0.05$) compared with BS 2.

Table 2 **Region-level analysis**

	Optimistic analysis			
	Sensitivity (95% CI)	Specificity (95% CI)	Accuracy (95% CI)	AUC (95% CI)
BS 1	49% (39–59%)	100% (99–100%)	93% (91–95%)	0.74 (0.71–0.77)
BS 2	54% (44–64%)	99% (98–100%)	93% (91–95%)	0.77 (0.74–0.80)
RBS 1	50% (40–60%)	98% (97–99%)[a]	92% (90–94%)	0.74 (0.71–0.77)
RBS 2	46% (36–56%)	98% (97–99%)[a,b]	91% (89–93%)	0.72 (0.69–0.75)
	Pessimistic analysis			
	Sensitivity (95% CI)	Specificity (95% CI)	Accuracy (95% CI)	AUC (95% CI)
BS 1	61% (51–71%)	97% (96–98%)	92% (90–94%)	0.79 (0.76–0.82)
BS 2	66% (56–75%)	94% (92–95%)	90% (88–92%)	0.80 (0.77–0.83)
RBS 1	70% (60–79%)[a]	89% (86–91%)[a,b]	86% (84–88%)	0.79 (0.76–0.82)
RBS 2	68% (58–77%)	84% (81–87%)[a,b]	82% (79–85%)	0.76 (0.73–0.79)

AUC, area under receiver-operating characteristic curve; BS 1, bone scintigraphy reader 1; BS 2, bone scintigraphy reader 2; CI, confidence interval; RBS 1, reprojected bone SPECT/CT reader 1; RBS 2, reprojected bone SPECT/CT reader 2.
[a]Statistically significant difference ($P < 0.05$) compared with BS 1.
[b]Statistically significant difference ($P < 0.05$) compared with BS 2.

Table 3 **Lesion-level analysis**

	Number of positive lesions reported	Number of true positive lesions	Detection rate of true positive lesions (%)	Number of false positive lesions	Number of false negative lesions	Number of equivocal lesions reported	Ratio of equivocal to all detected lesions (%)
BS 1	135	134	51	1	131	43	24
BS 2	176	169	64	7	96	62	26
RBS 1	163	144	54	19	121	139	46
RBS 2	163	137	52	26	128	185	53

reported positive by at least one RBS reader. All three patients who were falsely reported negative by both RBS readers were also falsely reported negative by both BS readers.

Ten regions were falsely reported negative by both BS readers but correctly positive or equivocal by at least one RBS reader. Three regions were falsely reported negative by both RBS readers but equivocal by at least one BS reader. No regions were falsely reported negative by both RBS readers but correctly positive by a BS reader.

The number of true positive lesions was similar between BS and RBS, but false-positive and equivocal lesions were more numerous in RBS images. The number of all malignant and equivocal lesions reported by each reader and their concordance with the reference standard diagnosis are shown in Table 3. Figures 1–3 contain visual comparisons of BS and RBS.

The CNR values measured from the femur, lumbar vertebra, and the tenth rib were on average, respectively, 175, 114 and 185% higher in RBS images than BS images. The

mean (SD) image quality grades given by the readers were 3.3 (0.7), 3.8 (0.5), 2.4 (0.6), 2.3 (0.6) for BS reader 1, BS reader 2, RBS reader 1 and RBS reader 2, respectively.

The patient-level inter-reader agreement values (95% CI) in the optimistic analysis were 0.75 (0.60–0.91) and 0.73 (0.59–0.88) for BS and RBS, respectively, and 0.57 (0.42–0.71) and 0.31 (0.15–0.48) for BS and RBS, in the pessimistic analysis, respectively.

Discussion

We compared RBS and traditional BS in terms of diagnostic performance and image quality. To our knowledge, this is the first study to compare diagnostic performance of RBS and BS in multiple patients using multimodal imaging and follow-up data as a reference standard. The RBS method has been presented earlier [7,10], but its diagnostic performance has not been validated. In this study, it was shown that, for the detection of bone metastases, the sensitivity of RBS surpasses that of BS at the cost of lower specificity.

When transitioning from BS to whole-body bone SPECT/CT, RBS can be a helpful tool. It has the familiar appearance of traditional BS combined with the improved lesion visibility of SPECT. Indeed, RBS seems so sensitive that the probability of missing a relevant lesion in RBS and finding it in SPECT would be low. The patient-level sensitivity of RBS in the pessimistic analyses of the current study ranged from 85 to 88%, while corresponding sensitivity of SPECT/CT in previous studies ranged from 63 to 95% [11,12]. The high sensitivity of RBS resulted in numerous equivocal findings, which, however, could be confirmed in clinical routine using the more specific SPECT/CT images which are available among RBS images. The specificity of SPECT/CT has been reported to be as high as 98% [11,12]. The specificity of RBS should also improve as the readers become more familiar with the appearance of detailed RBS images.

Fig. 1

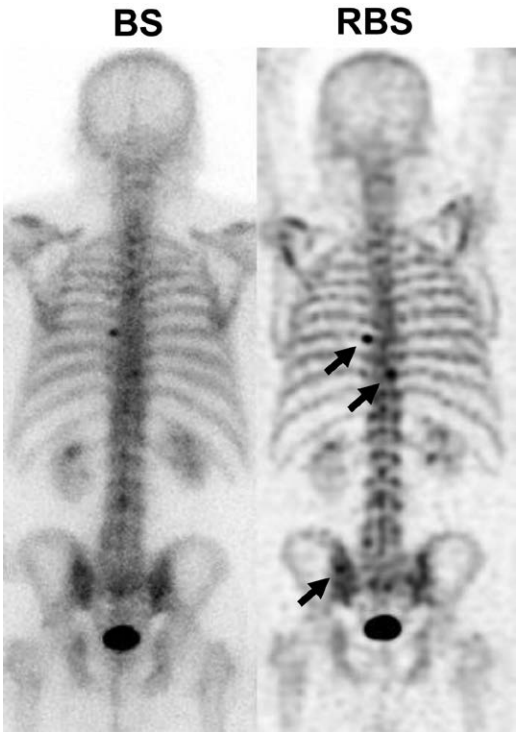

Posterior views of BS and RBS of a 77-year-old prostate cancer patient with bone metastases in the spine and pelvis. The patient was correctly reported positive by both RBS readers but falsely reported negative by one BS reader and equivocal by the other.

The reading of an RBS is more straightforward than the reading of a whole-body SPECT/CT, as an RBS consists of only two projections whereas a whole-body SPECT/CT consists of hundreds of slices. When the reading physician has access to both the RBS and whole-body SPECT/CT of the patient, he or she might begin the reading from the RBS images and use the SPECT/CT images to confirm the findings visible in RBS images.

We used only anterior and posterior views of RBS, but multiple views over a 360° rotation can also be reprojected. These reprojections could function as a physically more accurate rotating representation of SPECT images than the currently used MIP images, further improving the quality of the image reading process.

The image quality of RBS is affected by the acquisition and reconstruction parameters of SPECT. We used a rather fast SPECT/CT acquisition protocol suitable for clinical routine use. Also, all the SPECT corrections (attenuation, scatter and collimator response) being provided by the reconstruction software, iterations and subsets used in our clinical routine, and a rather narrow postprocessing filter were employed. These reconstruction parameters were optimized for SPECT/CT images and produced RBS images that were more detailed than traditional BS images and had more numerous and intense focal uptakes.

However, the increase in detail turned out to be counterproductive in this study, as the RBS images produced many equivocal findings not reported from BS images (Table 3). These equivocal findings mainly caused RBS to have higher sensitivity than BS, as the sensitivities of RBS and BS are more similar in the optimistic analyses where the equivocal findings were omitted. Especially, the three positive patients, who were detected by RBS but not by BS, had only equivocal findings in RBS. These patients were rated as true positive for metastases on patient and region levels although on lesion level some findings turned out to be false positive. This means that they were not the same lesions as the actual bone

Fig. 2

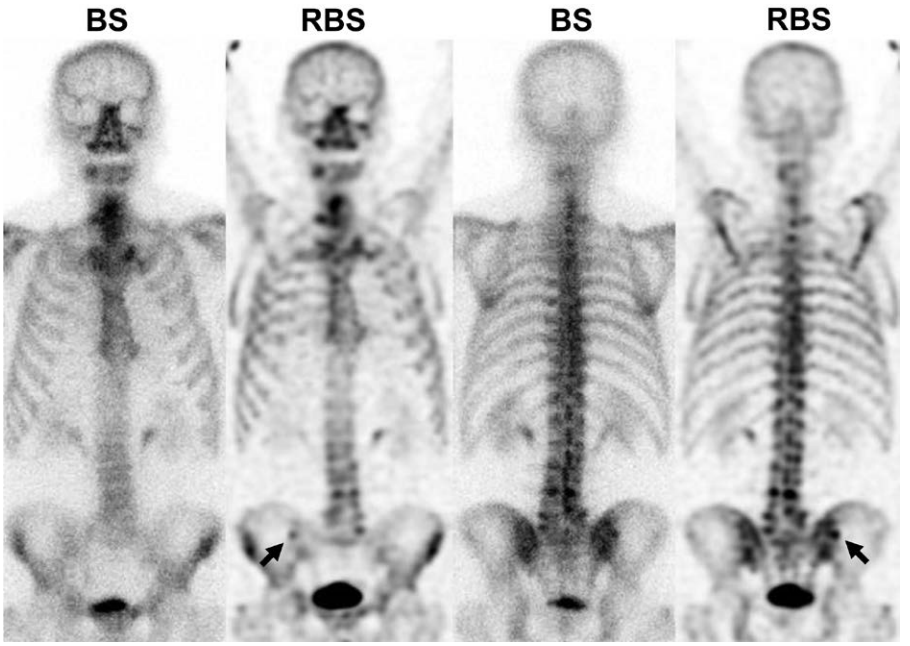

Anterior and posterior views of BS and RBS of a 72-year-old prostate cancer patient with bone metastasis in the pelvis. The patient was correctly reported positive by both RBS readers but falsely reported negative by one BS reader and equivocal by the other.

Fig. 3

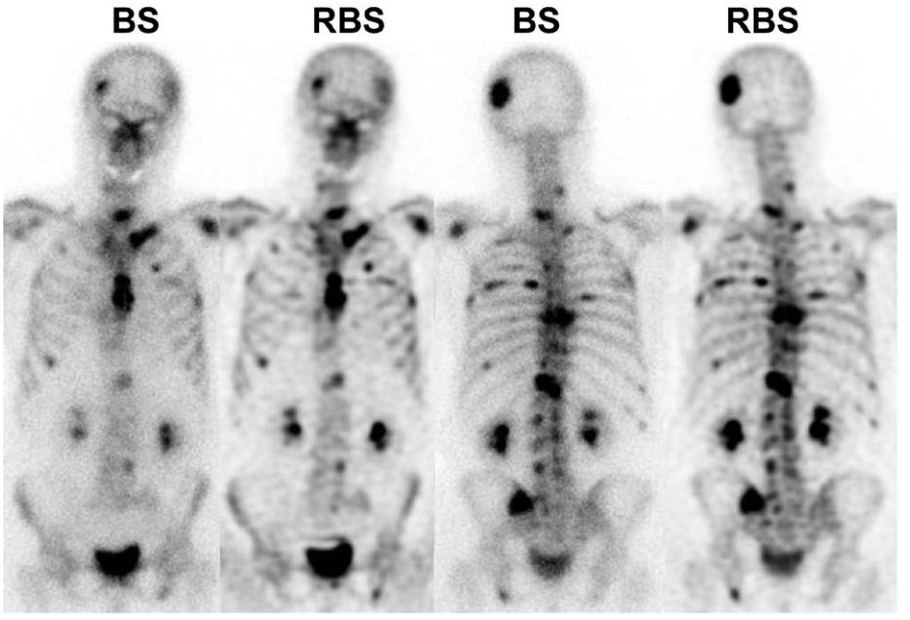

Anterior and posterior views of BS and RBS of a 75-year-old breast cancer patient with widespread bone metastases. The patient was correctly reported positive by all readers.

metastases detected only by DW-MRI, ^{18}F-NaF PET/CT or ^{18}F-PSMA-1007 PET/CT. These represent typical examples where increased sensitivity of RBS may also produce false-positive readings.

In retrospect, it might have been suitable to use a less complex SPECT reconstruction for RBS images, that is, lower resolution by using fewer iterations and omitting corrections for scatter and collimator response and

postprocessing filtering. This could have caused RBS images to appear even more like traditional BS images (Fig. 4). However, this would have also lowered the sensitivity of RBS closer to that of BS.

Image quality grades given by the reading physicians and interobserver repeatability were higher for BS than RBS. This also reflects the confusing amount of detail in RBS images. It must be emphasized, however, that while all our readers were experienced in reading BS images, they had no prior experience regarding RBS images. This may have diminished the image quality grades and specificity results of RBS and increased the number of equivocal findings, which is expected to decrease as the readers gain more experience on RBS images. At the same time, the reading of RBS images becomes faster and more reliable than now.

Nonetheless, RBS images had clearly higher CNR, which was caused by the higher contrast between bone and soft tissue and the smoother appearance of normal bone tissue. The CNR results therefore further highlight the higher sensitivity of RBS compared to BS images.

In this study, two different SPECT/CT systems were used, a digital system with CZT semiconductor detectors and an analogical system with NaI scintillation crystal detectors. However, the effects of detector technology on diagnostic performance could not be evaluated, because the patients examined using the different systems were different.

BS images are usually acquired within approximately 20 min. When considering the replacement of planar BS with whole-body bone SPECT/CT acquisitions and RBSs in clinical routine, the acquisition time of SPECT should be optimized. Current SPECT guidelines recommend 60–64 views and a 10–30 s acquisition time per view [20], which cause a three-bed SPECT/CT examination to last at least 40 min when camera head and bed movements are taken into account. We generated RBS images from resampled data corresponding to an optimized SPECT acquisition protocol with 60 views and 7 s per view and a total examination time of 30 min. Recently even faster bone SPECT acquisitions have been reported feasible, as next-generation gamma cameras are capable of acquiring whole-body bone SPECT/CTs in less than 20 min [7,21]. Therefore, in the near future, a 20-min whole-body SPECT/CT and RBS acquisition can be clinical routine.

The use of over-detailed RBS images may be regarded as a limitation of this study, as we used a reconstruction protocol optimized for SPECT/CT. The usage of different reconstruction protocols and postprocessing filtering could have changed our results, especially by reducing the number of equivocal findings. Our readers were also inexperienced regarding these sensitive RBS images. Our results showed the high sensitivity of the RBS method, and the specificity of RBS is expected to increase as the readers gain experience. Also, the optimal parameters for acquisition and reconstruction of RBS should be investigated in the future.

Fig. 4

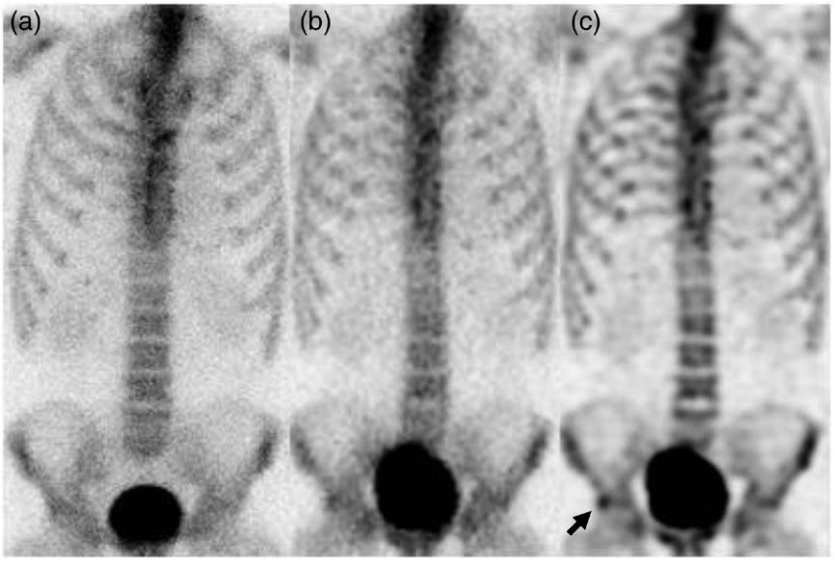

An example of a false positive finding caused by the more complex processing of RBS images. Anterior views of a BS (a) and two differently processed RBSs (b, c) of a 70-year-old prostate cancer patient. The first RBS (b) was reconstructed using 4 iterations and 15 subsets and without resolution recovery or filtering. The second RBS (c) was reconstructed similarly as images in this study using 6 iterations, 15 subsets and resolution recovery and a Gaussian filter with 7-mm full width at half maximum. The benign pelvis lesion marked with an arrow was falsely reported positive by one RBS reader and equivocal by the other.

Conclusion

Whole-body bone SPECT/CT can be reprojected into more familiar anterior and posterior planar images with excellent sensitivity for bone metastases with no need for additional acquisition of planar BS.

Acknowledgements

Conflicts of interest

A.S. has a consulting agreement with HERMES Medical Solutions. S.A. has received funding from Emil Aaltonen Foundation, Turku University Hospital and Turku University Foundation. For the remaining authors, there are no conflicts of interest.

References

1 Savelli G, Maffioli L, Maccauro M, De Deckere E, Bombardieri E. Bone scintigraphy and the added value of SPECT (single photon emission tomography) in detecting skeletal lesions. *Q J Nucl Med* 2001; **45**:27–37.

2 Rager O, Nkoulou R, Exquis N, Garibotto V, Tabouret-Viaud C, Zaidi H, *et al*. Whole-body SPECT/CT versus planar bone scan with targeted SPECT/CT for metastatic workup. *Biomed Res Int* 2017; **2017**:7039406.

3 Arvola S, Jambor I, Kuisma A, Kemppainen J, Kajander S, Seppänen M, Noponen T. Comparison of standardized uptake values between 99mTc-HDP SPECT/CT and 18F-NaF PET/CT in bone metastases of breast and prostate cancer. *EJNMMI Res* 2019;**9**:6.

4 Bailey DL, Willowson KP. An evidence-based review of quantitative SPECT imaging and potential clinical applications. *J Nucl Med* 2013; **54**:83–89.

5 Abikhzer G, Gourevich K, Kagna O, Israel O, Frenkel A, Keidar Z. Whole-body bone SPECT in breast cancer patients: the future bone scan protocol? *Nucl Med Commun* 2016; **37**:247–253.

6 Ljungberg M, Pretorius PH. SPECT/CT: an update on technological developments and clinical applications. *Br J Radiol* 2018; **91**:20160402.

7 Melki S, Chawki MB, Marie PY, Imbert L, Verger A. Augmented planar bone scintigraphy obtained from a whole-body SPECT recording of less than 20 min with a high-sensitivity 360° CZT camera. *Eur J Nucl Med Mol Imaging* 2020; **47**:1329–1331.

8 Bailey DL, Schembri GP, Harris BE, Bailey EA, Cooper RA, Roach PJ. Generation of planar images from lung ventilation/perfusion SPECT. *Ann Nucl Med* 2008; **22**:437–445.

9 Kyrtatos PG, Navalkissoor S, Burniston M, Wagner T. Planar images reprojected from SPECT V/Q data perform similarly to traditional planar V/Q scans in the diagnosis of pulmonary embolism. *Nucl Med Commun* 2013; **34**:445–450.

10 Bandi P, Zsoter N, Wirth A, Luetzen U, Derlin T, Papp L. New workflows and algorithms of bone scintigraphy based on SPECT-CT. *Annu Int Conf IEEE Eng Med Biol Soc* 2012; **2012**:5971–5974.

11 Jambor I, Kuisma A, Ramadan S, Huovinen R, Sandell M, Kajander S, *et al*. Prospective evaluation of planar bone scintigraphy, SPECT, SPECT/CT, 18F-NaF PET/CT and whole body 1.5T MRI, including DWI, for the detection of bone metastases in high risk breast and prostate cancer patients: SKELETA clinical trial. *Acta Oncol* 2016; **55**:59–67.

12 Anttinen M, Ettala O, Malaspina S, Jambor I, Sandell M, Kajander S, *et al*. A prospective comparison of 18F-prostate-specific membrane antigen-1007 positron emission tomography computed tomography, whole-body 1.5 T magnetic resonance imaging with diffusion-weighted imaging, and single-photon emission computed tomography/computed tomography with traditional imaging in Primary Distant Metastasis Staging of Prostate Cancer (PROSTAGE). *Eur Urol Oncol* 2021;**4**:635–644.

13 Lecouvet FE, Geukens D, Stainier A, Jamar F, Jamart J, d'Othée BJ, *et al*. Magnetic resonance imaging of the axial skeleton for detecting bone metastases in patients with high-risk prostate cancer: diagnostic and cost-effectiveness and comparison with current detection strategies. *J Clin Oncol* 2007; **25**:3281–3287.

14 Lecouvet FE, El Mouedden J, Collette L, Coche E, Danse E, Jamar F, *et al*. Can whole-body magnetic resonance imaging with diffusion-weighted imaging replace Tc 99m bone scanning and computed tomography for single-step detection of metastases in patients with high-risk prostate cancer? *Eur Urol* 2012; **62**:68–75.

15 Calais J, Ceci F, Eiber M, Hope TA, Hofman MS, Rischpler C, *et al*. 18F-fluciclovine PET-CT and 68Ga-PSMA-11 PET-CT in patients with early biochemical recurrence after prostatectomy: a prospective, single-centre, single-arm, comparative imaging trial. *Lancet Oncol* 2019; **20**:1286–1294.

16 Hofman MS, Lawrentschuk N, Francis RJ, Tang C, Vela I, Thomas P, *et al*; proPSMA Study Group Collaborators. Prostate-specific membrane antigen PET-CT in patients with high-risk prostate cancer before curative-intent surgery or radiotherapy (proPSMA): a prospective, randomised, multicentre study. *Lancet* 2020;**395**:1208–1216.

17 Hudson HM, Larkin RS. Accelerated image reconstruction using ordered subsets of projection data. *IEEE Trans Med Imaging* 1994; **13**:601–609.

18 Bexelius T, Sohlberg A. Implementation of GPU accelerated SPECT reconstruction with Monte Carlo-based scatter correction. *Ann Nucl Med* 2018; **32**:337–347.

19 Hanley JA, McNeil BJ. A method of comparing the areas under receiver operating characteristic curves derived from the same cases. *Radiology* 1983; **148**:839–843.

20 Van den Wyngaert T, Strobel K, Kampen WU, Kuwert T, van der Bruggen W, Mohan HK, *et al*; EANM Bone & Joint Committee and the Oncology Committee. The EANM practice guidelines for bone scintigraphy. *Eur J Nucl Med Mol Imaging* 2016; **43**:1723–1738.

21 Gregoire B, Pina-Jomir G, Bani-Sadr A, Moreau-Triby C, Janier M, Scheiber C. Four-minute bone SPECT using large-field cadmium-zinc-telluride camera. *Clin Nucl Med* 2018; **43**:389–395.